Ion-to-ion amplification through an open-junction ionic diode

Seung-Min Lim[a], Hyunjae Yoo[a], Min-Ah Oh[b], Seok Hee Han[b], Hae-Ryung Lee[a], Taek Dong Chung[b,c], Young-Chang Joo[a,d], and Jeong-Yun Sun[a,d,1]

[a]Department of Materials Science & Engineering, Seoul National University, 08826 Seoul, Republic of Korea; [b]Department of Chemistry, Seoul National University, 08826 Seoul, Republic of Korea; [c]Electrochemistry Laboratory, Advanced Institutes of Convergence Technology, 16229 Suwon-Si, Gyeonggi-do, Republic of Korea; and [d]Research Institute of Advanced Materials, Seoul National University, 08826 Seoul, Republic of Korea

Edited by John A. Rogers, Northwestern University, Evanston, IL, and approved May 29, 2019 (received for review March 6, 2019)

As biological signals are mainly based on ion transport, the differences in signal carriers have become a major issue for the intimate communication between electrical devices and biological areas. In this respect, an ionic device which can directly interpret ionic signals from biological systems needs to be designed. Particularly, it is also required to amplify the ionic signals for effective signal processing, since the amount of ions acquired from biological systems is very small. Here, we report the signal amplification in ionic systems as well as sensing through the modified design of polyelectrolyte hydrogel-based ionic diodes. By designing an open-junction structure, ionic signals from the external environment can be directly transmitted to an ionic diode. Moreover, the minute ionic signals injected into the devices can also be amplified to a large amount of ions. The signal transduction mechanism of the ion-to-ion amplification is suggested and clearly verified by revealing the generation of breakdown ionic currents during an ion injection. Subsequently, various methods for enhancing the amplification are suggested.

ionic diode | ionic signal amplification | polyelectrolyte gel | ionic circuit element

Beyond the wearable devices inspired by current stretchable electronics, more interactive devices are being incorporated into human bodies. In particular, the implementation of bio-integrated devices (1–6) that can sense and transmit signals from biological systems has resulted in their use in a wide range of applications, such as monitoring neural (7–10) or cardiac (11, 12) activities and delivering drugs (13–15) for medical care.

To date, biological signals have been acquired by electronic devices which are using metal electrodes (16, 17) or conjugated electroactive polymers (18–20). However, since the signals from a biological system are mainly based on transportation of ions (i.e., K^+, Ca^{2+}, neurotransmitters, etc.), a fundamental mismatch of signal carriers between electrical devices and biological system has made direct communication persistently difficult due to a high impedance created at the interfaces (16, 18). Therefore, an ion-based signal sensing system which can directly interpret ion signals from a biological system is required to promote the human–machine interfaces (21–23).

Considering the abovementioned issues, hydrogels have been extensively studied as a promising candidate of ionic conductors (21, 23–25) due to their inherent mechanical flexibility (15, 26) and excellent biocompatibility (27, 28). Moreover, by introducing cross-linked polyelectrolyte gels (21, 23) composed of fixed charges on their polymeric chains, it is possible to mimic the behavior of p-type or n-type semiconductors because only counter ions that are oppositely charged on the polyanionic or polycationic backbones are mobile due to Donnan exclusion. More recently, by combining different types of polyelectrolyte gels, the operation of ion p–n junction diodes (29–31) and transistors (32–34) has been demonstrated.

Despite the many advances that have been made in developing ionic devices, obtaining an ionic signal directly without changing signal carriers has remained problematic for the following reasons. In previously reported ionic devices, diodes or transistors were developed to be operated by an external electrical bias (19, 22, 35) with mimicking the functions of electrical semiconductor devices. For example, ionic transistors were successfully operated to transmit a signal by applying external voltages to the gate (34, 36). However, because the devices were designed for external bias, it was very hard to apply external ion signals to the devices. A new design is required to attract external ion signals to an ionic device.

Furthermore, an effective signal processing requires an amplification of weak ionic signals because the amount of ions which are released from a biological system is very small (16, 37, 38). However, the physics of signal amplification in an ionic system has not been introduced yet, and it is very difficult to apply the mechanism of signal amplification for electrical semiconductors to an ionic system. For instance, a bipolar junction transistor can be activated when the diffusion length of the minority carrier in the emitter is large enough to cross the base region (39). However, such amplification is rather difficult to be achieved in an ionic system, because ions are relatively heavier than electrons, so that they have low mobility.

Here, we have developed an open-junction ionic diode (OJID) to transmit ionic signals directly. OJID is an ionic diode which is fabricated based on polyelectrolyte hydrogels as shown in Fig. 1*A*. Because OJID has a hole near the junction between p-type

Significance

For intimate communication between electrical devices and biological areas, signal transfer in human–machine interfaces has become an issue due to differences in signal carriers. Furthermore, as the amount of ions acquired from biological systems is very small, amplification of weak ionic signals is required for effective signal processing. Here, we report the signal amplification effect observed in a fully ionic device system. Through the modified design of polyelectrolyte gel-based ionic diodes, minute ionic signals can be directly injected into ionic devices and can also be amplified to a large amount of ions by generating additional ionic currents. Our findings will be applicable to engineering ion-based information processing devices, as well as achieving direct communication with biological signals.

Author contributions: S.-M.L., T.D.C., Y.-C.J., and J.-Y.S. designed research; S.-M.L., H.Y., M.-A.O., S.H.H., and H.-R.L. performed research; S.-M.L., H.Y., M.-A.O., S.H.H., T.D.C., Y.-C.J., and J.-Y.S. analyzed data; and S.-M.L. and J.-Y.S. wrote the paper.

The authors declare no conflict of interest.

This article is a PNAS Direct Submission.

[1]To whom correspondence may be addressed. Email: jysun@snu.ac.kr.

This article contains supporting information online at www.pnas.org/lookup/suppl/doi:10.1073/pnas.1903900116/-/DCSupplemental.

Published online June 20, 2019.

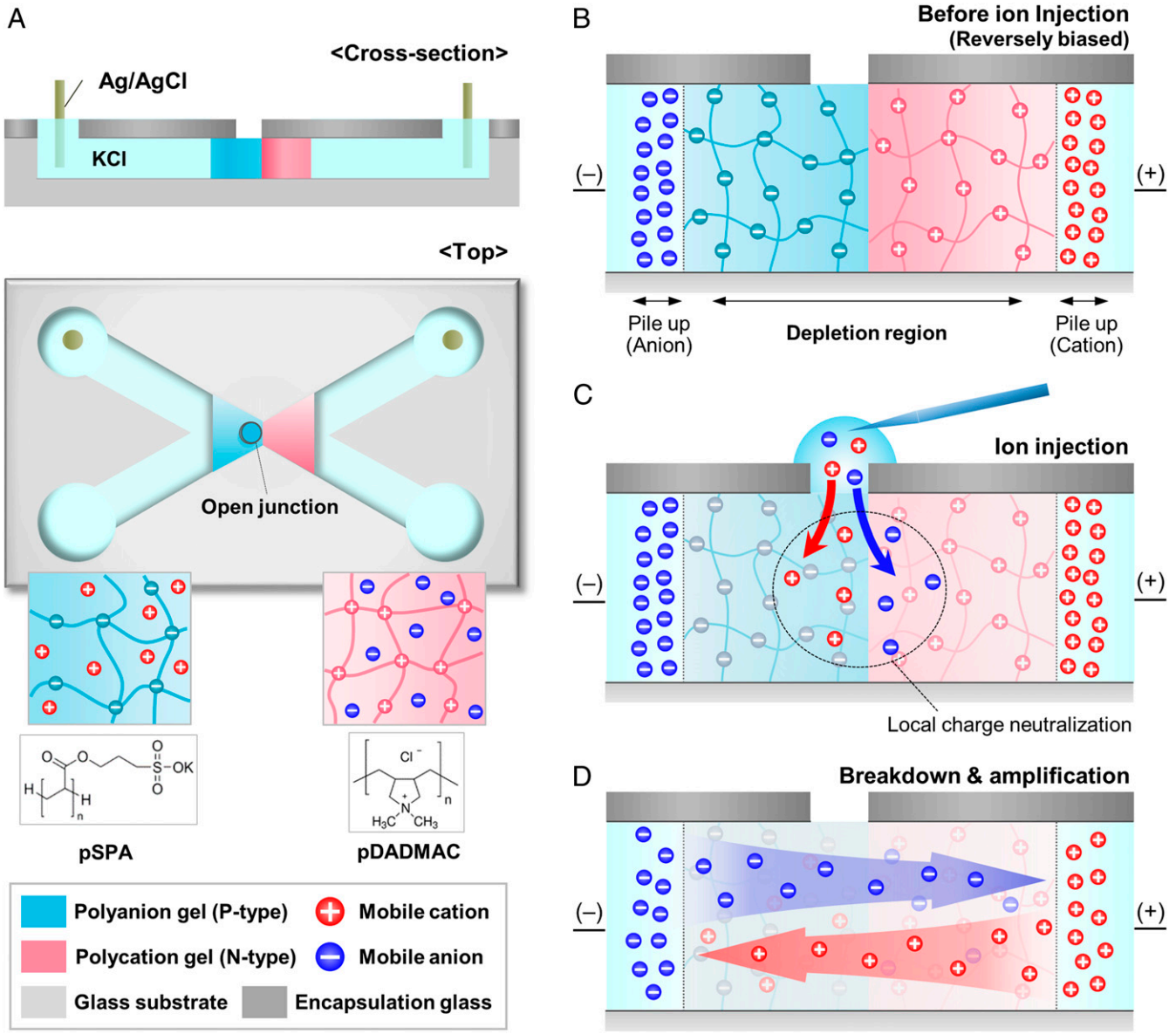

Fig. 1. Basic design of OJIDs and principle of ion-to-ion amplification. (*A*) Schematic representation of an OJID. Through the ion-injectable hole structure formed on the polyelectrolyte gel region, ionic signals can be directly transmitted to the active element of devices. (*B–D*) Suggested signal amplification mechanism by ion injection. (*B*) In the reverse-biased state of an OJID, the depletion region is formed in the diode, and mobile ions in the reservoir are piled up at reservoir/gel interfaces by charge repulsion. (*C*) When an ion is injected through the open junction, local charge neutralization in the diode occurs, and in addition to the injected ions, (*D*) an additional breakdown current from the reservoir can be observed.

and n-type hydrogels, a signal of ions from the external environment can be directly injected through the hole into the junction. During an operation of OJID, an amplification of ion signal was observed. The mechanism of the ion-to-ion signal amplification was suggested and verified by revealing the generation of the breakdown ionic currents crossing over the diode during ion injections through experimental and computational studies. A way to enhance the amplification performance of OJIDs was suggested through the systematic studies of parameters.

Results and Discussion

Design of OJID. The fabrication process and representative architecture of OJIDs are illustrated in Fig. 2 *A* and *B*. By introducing D263 ultrathin borosilicate glass (~30 μm, Schott) as an encapsulation layer of microfluidic channels, which is amenable to laser hole drilling, an ion-injectable microhole (d ~ 50 μm) could be formed and aligned with the p–n junction interface (*SI Appendix*, Fig. S1). After fabricating microfluidic glass chips, n-type poly(diallyl-dimethylammonium chloride) (pDADMAC) and p-type poly(3-sulfopropyl acrylate potassium salt) (pSPA) polyelectrolyte gels were sequentially patterned on the microfluidic chip by UV photopolymerization (*SI Appendix*, Fig. S2). Subsequently, channels in the microfluidic chip were filled with reservoir ionic solution for the dialysis of polyelectrolyte gels and the formation of electrochemical contact. To apply a reverse bias to the OJIDs and measure the responsive ionic current signal without potential loss, nonpolarizable Ag/AgCl electrodes were connected to both sides of the reservoir. A picoliter microinjector (Warner instruments) was used to deliver ions locally to the microhole region (Fig. 2 *C* and *D* and Movie S1). By modulating injection parameters such as the injection pressure and time, as

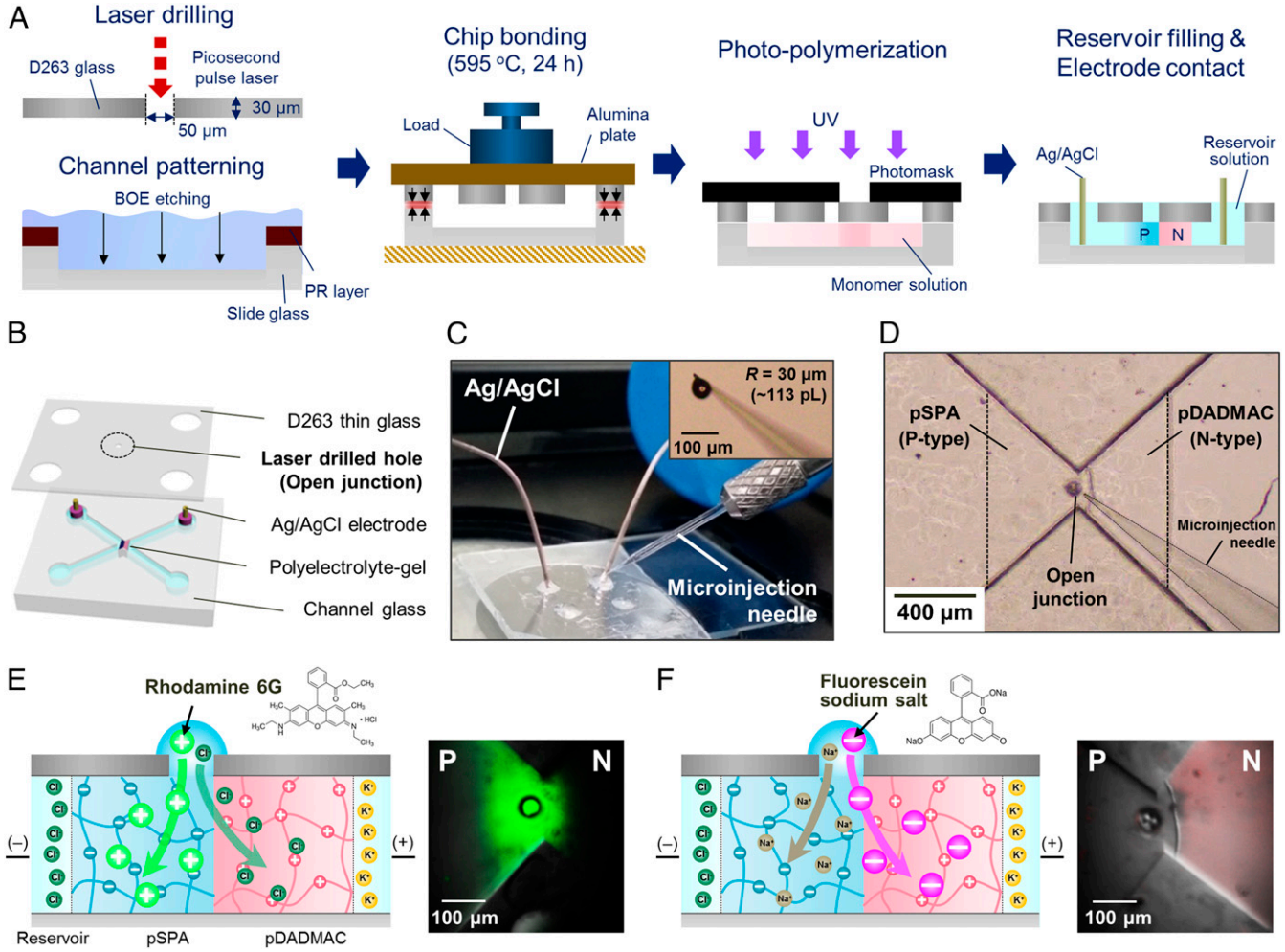

Fig. 2. Fabrication of an OJID and ion injection system. (*A*) Fabrication process and (*B*) architecture of an OJID in a microfluidic chip. By introducing thin glass (~30 μm) as an encapsulation layer, an ion-injectable microhole could be patterned on the devices. (*C*) Device configuration for ion injection. The volume of injected ionic solution was precisely controlled using a picoliter injector. Nonpolarizable Ag/AgCl electrodes were connected to the reservoir for in situ current measurement upon ion injection. (*D*) Microscopy images of OJID before ion injection. (*E* and *F*) Schematic illustrations and fluorescence images indicating how the distribution of injected ions is monitored. (*E*) After the injection of the Rhodamine 6G fluorescent cations, most of the green fluorescence was observed in the pSPA region. (*F*) The injected fluorescent sodium salt anions were observed in the pDADMAC region, indicating ion injection into the devices through the open junction.

well as the inner diameter of the microneedle, the diameter of the injected ionic solution droplets was precisely controlled (Fig. 2 *C*, *Inset*), and the amount of charge in the ionic input signal could also be quantified.

To confirm whether both the positive and negative ions were injected into the OJIDs through the microhole, fluorescent ions (30) were injected into the devices to visualize the distribution of injected ions. Fig. 2 *E* and *F* shows fluorescence microscopy images of the ionic distribution of Rhodamine 6G cations (green) and fluorescein salt anions (red) after ion injection. Because the injected cationic and anionic fluorescent dyes were detected in the pSPA (p-type) and pDADMAC (n-type) regions, respectively, we verified that both the cations and anions were well injected into devices. Furthermore, we also found that there was no significant difference in the performance of the devices regardless of the position of the hole as long as it is located near the junction interface (*SI Appendix*, Fig. S3).

Verification of Ion-to-Ion Amplification Mechanisms. The proposed mechanism of the ion-to-ion amplification effect through the OJIDs is illustrated in Fig. 1 *B*–*D*. When reverse-bias voltages are applied to the OJIDs at the initial stage, counter mobile ions in the polyelectrolyte gels are depleted, and coions in the reservoir cannot be transported to the diodes because the repulsive force acts on the fixed ions in the polyelectrolyte gels and potential drops are mainly applied to the depletion region of the device rather than the gel/reservoir interfaces. Therefore, if the minute ionic solution is injected into the region adjacent to the p–n junction interface in the reverse-biased state, the ionic signal can be followed by the reverse current peak. In particular, as the depletion region in OJIDs is temporarily neutralized by injected ions through the open junction of the devices, the transport number of each polyelectrolyte gel can be lowered, and then, the coions at pile-up regions can transport into the gels, which results in an additional ionic current from the reservoir region. This phenomenon is similar to the breakdown current in electronics but replenishable in aqueous ionic systems.

To test our hypothesis that the breakdown ionic current occurs across the reservoir region due to local charge neutralization in the depletion region of OJIDs after ion injection through the microhole, selective fluorescent dyes (40) that emit fluorescence by reaction with a specific ion were utilized. The selective

reaction of Rhodamine B hydrazide (RBH) with the Cu^{2+} ion was used to observe the crossing current due to the cationic flux from the reservoir on the pDADMAC side (Fig. 3*A*). When the KCl solution including RBH was introduced into the pSPA side while $CuSO_4$ was introduced into the pDADMAC side and a reverse-bias voltage was applied, fluorescence was rarely detected due to the charge repulsion between fixed charges in the polyelectrolyte gels and counter mobile ions in the reservoir region. Interestingly, after injecting a KCl solution through the microhole in the OJIDs, a red fluorescence signal was observed at the KCl + RBH reservoir/pSPA interface, as shown in Fig. 3*B*; this finding implies that the Cu^{2+}-based ionic flux crossed over to the polyelectrolyte gels during KCl injection. Likewise, the anion-based breakdown current from the pDADMAC side was also confirmed by the observation of OH^- flux through the selective reaction of carboxy-fluorescein (cFlu) on the pDADMAC side reservoir, which showed cyan fluorescence under a basic environment after the injection of a KCl solution (Fig. 3 *C* and *D*). These results confirm that an additional amplification ionic current can occur during the temporary breakdown of the ionic diodes.

In addition to the visualization of the ion flux using selective fluorescence dyes, we performed finite-element method (FEM) simulation to investigate the generation of the breakdown ionic current crossing the diode using COMSOL Multiphysics. The physical models and their boundary conditions used for simulation are displayed in Fig. 3*E*. A 2D model was adopted to save computational resources, and the 2D geometry of the polyelectrolyte gels in the simulation was designed to be identical to that of the real devices. In the steady state under the reverse bias, it was assumed that the fully depleted state of the OJIDs could be attained, in which the regions of the pSPA and pDADMAC

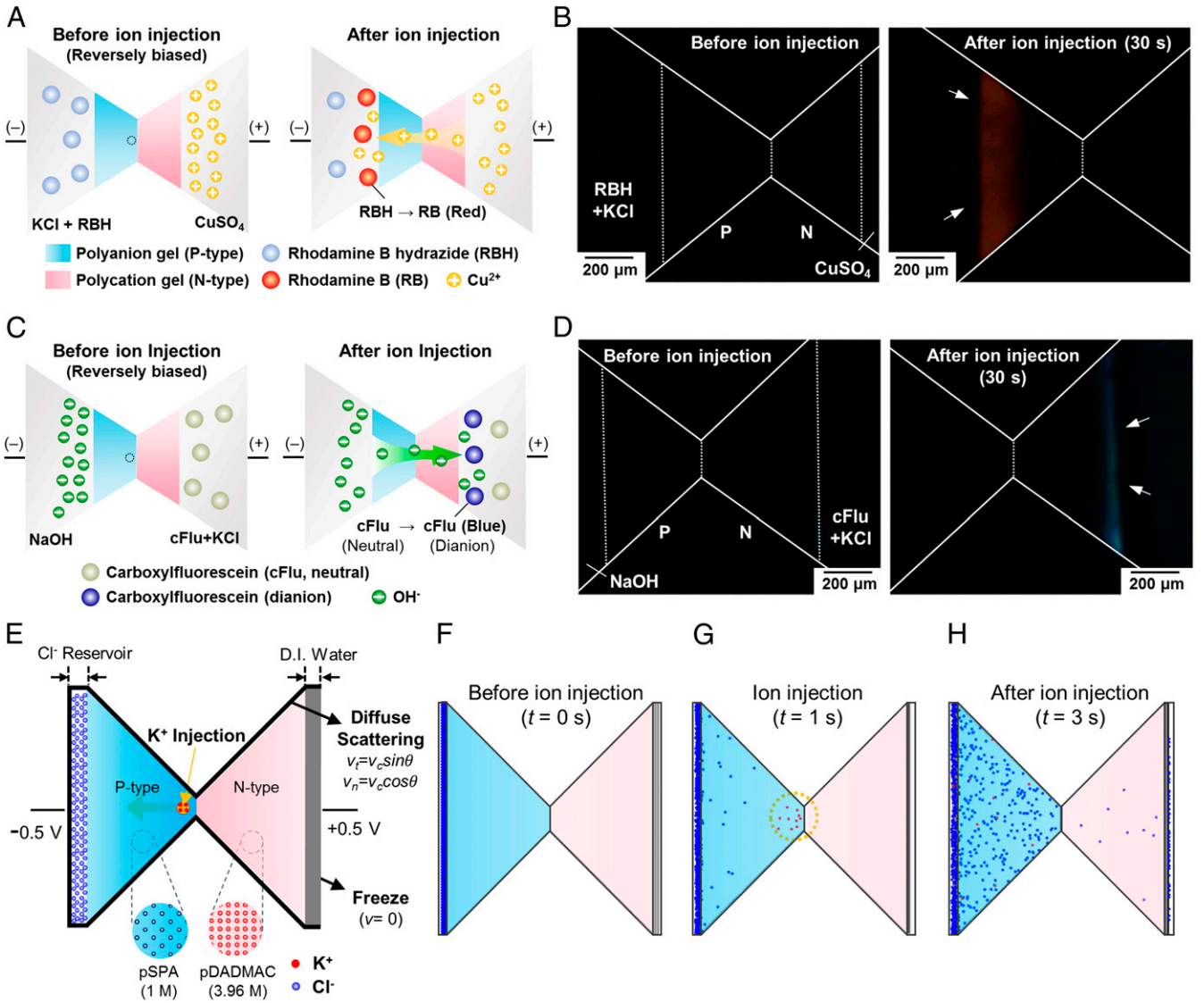

Fig. 3. Breakdown of the ionic diode by ion injection. Schematic depiction and images of fluorescence induced by (*A* and *B*) Cu^{2+} ion and (*C* and *D*) OH^- ion flux after ion injection. When Rhodamine B hydrazide (RBH) was incorporated into the reservoir on the pSPA side, red fluorescence emerged after KCl injection to the open junction, which was caused by the Cu^{2+} ion flux induced by the breakdown of the ionic diode. Likewise, as pH-sensitive cFlu dye was introduced into the reservoir on the pDADMAC side, OH^- based anionic flux was visualized through cyan fluorescence. (*E*) Two-dimensional model and boundary conditions for numerical calculation. (*F*) Before ion injection, Cl^- ions were piled up at the reservoir/gel interface by charge repulsion. (*G*) When ions were injected into the open junction at 1 s, charge neutralization in pSPA occurred locally, and (*H*) the breakdown current (Cl^- ion flux) could be observed on the reservoir side.

gels were only composed of anionic and cationic fixed charges, respectively. Additionally, the charge pile-up region at the gel/reservoir interface was designed by introducing a Cl^- accumulation layer on the pSPA side (detailed information regarding the FEM simulation is provided in *SI Appendix*).

Fig. 3 *F–H* and Movie S2 show the ion distributions in the gel diode during the ion-to-ion amplification. Considering the symmetric structure of the model, only the anionic (Cl^- ions) flux crossing the pSPA region was calculated using the charged particle tracing model. Before ion injection, most of the Cl^- ions in the reservoir held their positions because of the repulsion between Cl^- ions and fixed charges in the pSPA gel. However, when the K^+ ion particles were injected near the junction at $t = 1$ s, a small amount of injected K^+ ions activated Cl^- ions in the pile-up region, overcoming the repulsion between anionic fixed charges in the pSPA gel and passing to the pDADMAC gel region.

Electrochemical Characterization. Based on the verification of the ion-to-ion amplification mechanism in the OJIDs, various case studies were conducted to investigate the factors responsible for the modulation and improvement of the amplification effect in the devices. Fig. 4*A* presents the changes in the responsive ionic peak current after ion injection as a function of the concentration of the KCl reservoir. An in situ measurement of the breakdown current during ion injection was conducted by varying the ionic concentration of the KCl reservoir from 1 mM to 0.1 M, where the amount of the injected ion solution was fixed to KCl 0.1 M for 113 pL (Q ~2.16 μC). For quantitative analysis, the detected charge amount was measured through the integration of the reverse current peak in the *i-t* curve for 1 min from the onset of ion injection (Fig. 4*B*). When a sufficient depletion state was formed in the OJIDs by applying a reverse bias of −1 V for 3 min, the ionic current was well rectified, indicating only a low leakage current. After ion injection, the ionic signal response was observed in the form of the reverse current peak, as predicted. The onset and decay of ionic current peaks occurs during around 20~30 s for a diode with a width of 450 μm, which is quite different from the basic kinetics of a single polyelectrolyte hydrogel, showing the sharp response to the bias (*SI Appendix*, Fig. S5). This result indicates that an additional ionic current across the reservoir region can also be confirmed by an electrochemical signal.

For a KCl reservoir concentration of 1 mM, the amount of charge detected from the response current peak was measured to be 1.93 μC, which was similar to the charge of the injected ions. As the concentration of the KCl reservoir solution was increased to 0.01 and 0.1 M, however, a considerable increase in the reverse peak current was observed. Moreover, the detected charge amount also increased to 3.75 and 10.81 μC, respectively. These results suggest that the reservoir concentration is related to the concentration of coions in the pile-up regions, which also increases the potential drops at the gel/reservoir interface for the generation of a breakdown ionic current from the reservoir.

Additionally, the tendency between the reverse-bias voltage and the responsive ionic signal was also investigated, as shown in Fig. 4 *C* and *D*. When the reverse-bias voltage was varied from −0.5 to −2 V and the concentration of the KCl reservoir was set to 0.1 M, the level of the ionic current peak was increased and even sharpened; thus, an increase in the charge amount was observed. It can be inferred that the field increases between both sides of the reservoir, which accelerates the crossing current through the diodes during the temporary breakdown.

Furthermore, we inspected the change in the amplification current of the OJIDs by varying the cations in the constituent reservoir solution and injecting a corresponding solution. Fig. 4 *E* and *F* presents the signal characteristics map and calculated ionic charge amount with respect to the cation species in the reservoir and the variation in the injected ionic solution from KCl to NaCl and LiCl. Among the various types of cations constituting the reservoir ionic solution, the highest breakdown current peak was observed in the KCl reservoir-based diodes, and their amplification effect was progressively weakened in going from a NaCl to LiCl reservoir-based diode. The ion mobility of cations in the polyelectrolyte gels was concluded to have a great effect on the crossing of the diodes during the momentary neutralization of the diodes in the reverse-biased state. When cations are hydrated, water molecules are attracted to the charged ions, and the effective radius of alkali ions increases in the order of $K^+ < Na^+ < Li^+$ (*SI Appendix*, Table S1) (41), which leads to a decrease in mobility in polyelectrolyte gels. To confirm the difference in ion mobility with varying reservoir solution, ion conductivities were measured from the slope of the *I-V* sweep curve using the salt bridge model as described in *SI Appendix*, Fig. S4. The changes in ion conductivities in the pSPA and pDADMAC gels with different reservoir solutions are shown in Fig. 4*G*. In the case of the pSPA (p-type) gel, a decrease in ion conductivity was observed as the effective hydrated radius of the constituent cation increased. However, the ion conductivity in the pDADMAC (n-type) gel remained nearly unchanged with respect to the reservoir solution because the conduction of n-type gels is mainly caused by anions. However, we believe that the difference in ion mobility due to the difference in the effective hydrated radius of the cations could also be effective in crossing the n-type gel region from the reservoir during the breakdown of the diodes.

In addition to the change in the reservoir solution, the change in the responsive ionic peak current and the subsequent detected charge amount were confirmed by varying the species of injected ionic solutions. As the mobility of cations in injected ionic solutions decreased ($Li^+ < Na^+ < K^+$), a reduction in the amplification effect of the devices was observed. Such changes could be caused by the difference in the drift length of the cations in the polyelectrolyte gels for local charge neutralization when injected, which can be related to the activation of the amplification mechanism in the diodes.

Enhancement of Amplification Effect. Through the various case studies, it was verified that the amplification effect of the ion signal is systematically controllable by modulating the parameters related to the breakdown current in the diodes, such as the concentration of reservoir ionic solutions and the field applied between the reservoirs. Furthermore, additional improvement of the amplification effect can be expected with a decrease in the width of the constituent polyelectrolyte gels of the diodes. Fig. 5*A* presents the responsive characteristics maps of various OJIDs with respect to the width of the polyelectrolyte gels in the diodes. The width of both the pSPA and pDADMAC gels were modulated from 150 to 850 μm, and the reverse-bias voltages were varied from −0.5 to −2 V. As observed in each reverse-bias voltage condition, the intensity of the breakdown current was remarkably increased as the width of the gel constituting the diode decreased, indicating a significant improvement of the ion-to-ion amplification effect. However, when the width of the constituent gel was increased to 850 μm, the amplification effect of the devices was diminished, and the detected charge amount was close to that of the injected KCl ionic solution. These results strongly suggest that the decrease in the width of the constituent gels in the OJIDs is a key factor for inducing breakdown current by decreasing the crossing distance as well as increasing the field applied between the polyelectrolyte gels.

Additionally, it was observed that the transmittance times for the signal response were drastically reduced. Based on slow breakdown sequences, the OJID exhibits a long response time compared with the conventional electronic devices. For practical application of OJIDs to the biological signal sensing, it is

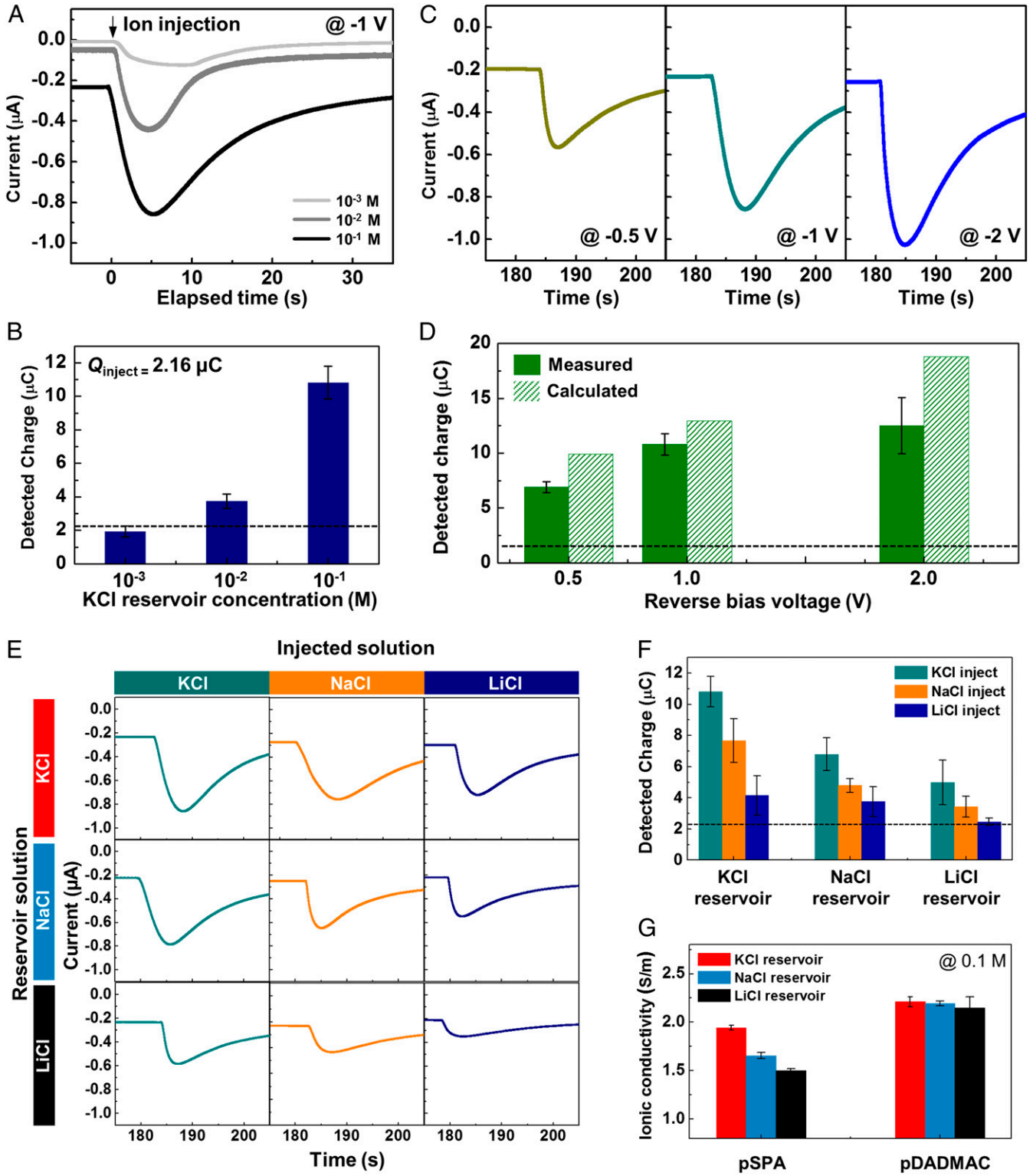

Fig. 4. Ion-to-ion signal amplification. Breakdown current began to flow when an ionic signal was injected and lasted for 20–30 s. The breakdown currents are influenced by the (*A* and *B*) reservoir concentration, (*C* and *D*) reverse-bias voltage, and (*E*–*G*) ion species. Dashed lines in *B*, *D*, and *F* represent the charge amount of injected ions. (*A*) When the ion concentration in the reservoir was increased from 1 mM to 0.1 M, a remarkable change in the breakdown current was measured, thus (*B*) increasing the charge amount detected from the current peak. Additionally (*C* and *D*), an additional increase in the breakdown currents was observed by varying the reverse-bias voltage conditions; this increase is related to the increase in the field applied to the diodes during breakdown. Additionally, the variation of the detected charge amount well matched the simulation results. (*E*) The breakdown current response map and (*F*) measured charge amount of various OJIDs considering the cations in the reservoir and injected ionic solutions. As the hydrated ionic radius increases ($K^+ < Na^+ < Li^+$), the ion mobility in the polyelectrolyte gels decreases, which yields different signal responses with varying constituent ions. This relationship was confirmed measuring (*G*) the change in the ionic conductivity in the pSPA gel with respect to the cations in the reservoir solutions.

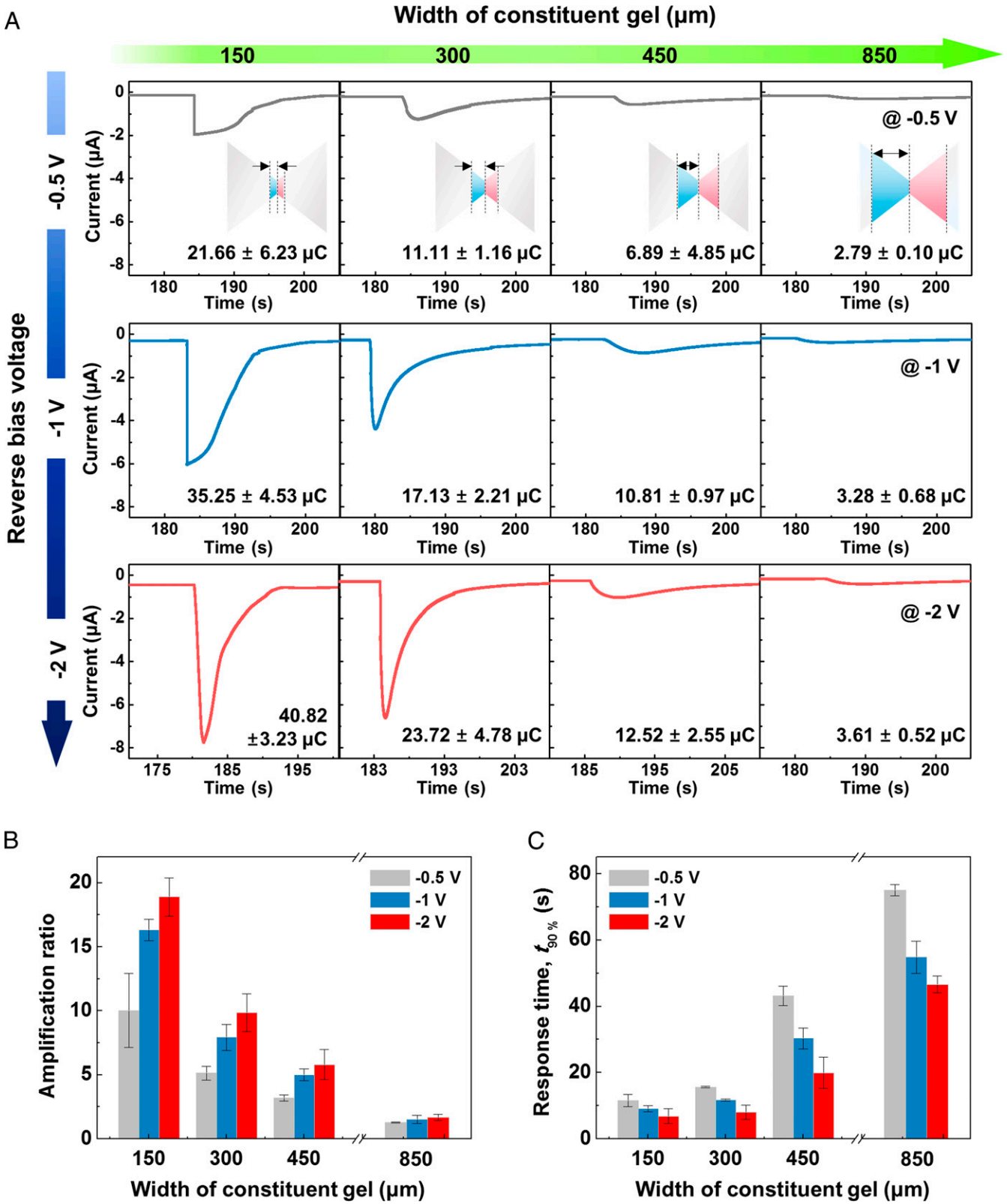

Fig. 5. Size effects for signal amplification. (*A*) Change in the responsive breakdown ionic current upon ion injection with respect to the dimensions of the constituent gels (150~850 μm) and reverse-bias voltage (−0.5 ~ −2 V). The concentrations of the reservoir solution and injected ionic solution were fixed to 0.1 M KCl. (*B*) Amplification ratio and (*C*) response time of OJIDs were significantly improved through the modulation of dimension of constituent gels and bias conditions.

required to shorten the response time of the devices. Therefore, we also analyzed the speed of OJIDs; the results are presented in Fig. 5*C*. The response time of OJIDs was quantified by the time that recovers 90% of initial currents ($t_{90\%}$) after ion injection (*SI Appendix*, Fig. S8). When the constituent gels and reverse-bias voltage of devices were set to 450 μm and −1 V, respectively, $t_{90\%}$ of the devices was measured to be approximately 30−40 s. However, as the width of the gel constituting the diode decreased to 150 μm, $t_{90\%}$ of the devices was significantly decreased below 10 s.

Along with the width of the diodes, an additional increase in the amplitude and sharpness of the response current peak was achieved as the reverse-bias voltage was increased to −2 V, which resulted in an improvement in the amplification ratio up to 18.9 times the charge amount of the injected KCl ionic solution (Fig. 5*B*). Further enhancement of the amplification performance as well as the speed of OJIDs can be expected through advances in the fabrication process for scaling down of devices.

Conclusions

In this study, we demonstrated unique sensing and amplification mechanisms based on the inherent features of ionic systems. By designing an ion-injectable structure in microfluidic chip-based ionic diodes, direct communication between an ionic input signal and ionic devices was facilitated without a gate bias in the medium. When an ionic solution is injected into the region adjacent to the interface of the p–n junction in the reverse-biased state, temporary breakdown in the diode can occur by the local charge neutralization in the depletion region at the polyelectrolyte gel junction, and an additional ionic current crossing over the diode from the reservoir can be generated in addition to the injected ionic signal. To verify the mechanisms of ion-to-ion signal amplification, the breakdown ionic flux was visualized using the ion-selective response of fluorescent dyes, which was also predicted by computational simulation. The signal amplification effect in OJIDs was successfully controlled by modulating the reservoir concentration, reverse-bias voltage, and ion species. Furthermore, a considerable increase in the breakdown current was observed by scaling down the polyelectrolyte gels, which resulted in an amplification factor of approximately 20 times in fully ion-transfer systems. We believe that our findings indicate future opportunities for fabricating signal-processing devices for ionic systems as well as for achieving intimate communication with biological signals.

Materials and Methods

Materials. All chemical reagents were used without further purification. Diallyldimethylammonium chloride (DADMAC), 3-Sulfopropyl acrylate potassium salt (SPA), *N,N′*-methylenebisacrylamide (cross-linker, MBAAm), 3-(trimethoxysilyl)propyl methacrylate (TMSMA), methanol, acetic acid, fluorescein sodium salt, Rhodamine 6G, RBH, Hepes, acetonitrile, cFlu, copper sulfate, sodium hydroxide, potassium chloride, sodium chloride, and lithium chloride were purchased from Aldrich. Lithium phenyl-2,4,6-trimethylbenzoylphosphinate (LAP) photoinitiator and Ag/AgCl electrodes were purchased from Tokyo Chemical Industry and CHI Instruments, respectively. The precursor solutions of the polyelectrolyte gels were aqueous and prepared with the following compositions: pDADMAC gel (n-type): 3.96 M DADMAC, 1 wt % MBAAm, 0.2 wt % LAP; and pSPA gel (p-type): 1 M SPA, 4 wt % MBAAm, 0.2 wt % LAP.

Fabrication of OJIDs. To design the open-junction structure for the injection of an ionic solution into the channel of the microfluidic chip, a microhole was formed at the p–n junction interface by laser hole drilling (KOS-SF1000RBS picosecond UV laser system, KORtherm Science), and openings for the reservoir were formed in the encapsulation glass layer [D263 ultrathin glass (=30 μm), Schott]. The channels in the glass substrate were patterned using photolithography and a wet-etching process following a previously reported procedure. Soda lime glass slides of hydrolytic class 3 with a thickness of 1 mm (Marienfeld) were used as substrates. After being cleaned with a piranha solution (H_2SO_4: H_2O = 3:1, J. T. Baker) to remove organic residues from the surfaces, the glass slides were rinsed with deionized water and then dehydrated on a hot plate at 175 °C for 10 min. The cleaned glass substrates were spin-coated (ACE-200, DongAh Trade Corp.) with hexamethyl-disilazane (Clariant) and AZ4620 photoresist (PR, Clariant), and soft baking was performed at 110 °C and 100 °C for 1 min 30 s. After alignment with a channel-patterned mask, the PR layer was exposed to UV light with an intensity of 21 $mWcm^{-2}$ for 20 s (MDE-4000, Midas) and then developed with an AZ 400 K developer (Clariant) for 1 min 30 s. The PR-patterned glasses were annealed on a hot plate at 180 °C for 15 min for hard baking and then etched with a 6:1 buffered oxide etch solution (J. T. Baker). As the rate of glass etching was confirmed to be 0.8 μm/min, channels in the glass with a highly uniform depth of 50 μm depth could be achieved. After alignment of the microholes in D263 glass and the center of the channel in patterned slide glass, the 2 glass surfaces were thermally bonded (595 °C for 18 h) under a 200 g load for encapsulation.

To form a polyelectrolyte gel junction in the microfluidic chip, the channel was treated with a mixture of TMSMA, acetic acid, and methanol (the ratio of the solution mixture was 1:2:2) for 1 h to enable stable adhesion between the polyelectrolyte gel and glass and then cleaned with methanol. Due to the surface tension of the gel precursor solutions and mechanical instability of cured gels during suction, it is difficult to form a hole at the junction interface. In this study, we first formed the pDADMAC gel at the outer region of hole and filled the other region including the hole with the pSPA gel.

First, whole channels in a microchip were filled with the precursor solution of the pDADMAC gel using a micropipette. The channel in the microfluidic chip was aligned with the photomask and exposed to UV light with an intensity of 21 $mWcm^{-2}$ for 2.5 s (MDE-4000, Midas), and then, the uncured precursor solution was removed through a suction tube. Subsequently, photopolymerization of the pSPA gel was performed using the same method, except that the exposure time under UV light was 3 s. As the both pDADMAC and pSPA precursor solutions include the same initiator and cross-linker, the pSPA gel was well formed adjacent to the pDADMAC gel through the sequential photopolymerization without generating gaps at junction. After being washed with KCl solution several times, the fabricated ionic diodes were stored in 0.1 M KCl solution for more than 1 d before characterization.

Electrochemical Characterization of Ion-to-Ion Amplification. To characterize the response ionic signal after ion injection, an in situ measurement of the ionic current was conducted using an electrochemical analyzer (MP3, ZIVE) with a constant reverse bias on the ionic diodes. After the formation of a fully depleted state in the polyelectrolyte gel diodes, under a constant reverse current, ionic solution (0.1 M KCl, NaCl, LiCl) was injected into the open junction of the microfluidic chip through a microinjection needle connected to a picoliter microinjector (PLI-100A, Warner instruments). The microinjection needle was produced by pulling glass capillaries (GC100-10, Harvard Apparatus) with a dual-stage glass micropipette puller (PC-10, Narishige). To protect the tip of the microinjection needle during filling, which is vulnerable to high pressure, ionic solutions were back-filled by inserting a nonmetallic microsyringe (Microfil, World Precision Instruments) into the microinjection needles. The volume of injected ions was calibrated by controlling the injection pressure and time pulse of the picoliter microinjector.

Optical Measurements. The distribution of injected ions was visualized using charged fluorescent dyes. After injecting cationic and anionic fluorescent dye solutions through the open junction of devices (10 μM Rhodamine 6G and 10 μM fluorescein sodium salt, each), fluorescence images were observed. To investigate the additional ion flux caused by ion injection, RBH and cFlu dyes were utilized, which are selectively responsive to Cu^{2+} and OH^-, respectively. An RBH concentration of 50 μM was employed in the 0.1 M KCl reservoir on the pSPA side with 0.1 M Hepes buffer (pH 7.0, 80%) and acetonitrile (20%). Additionally, 50 μM cFlu was adopted in the KCl reservoir on the pDADMAC side. The concentrations of $CuSO_4$ and NaOH were set to 0.1 M. The fluorescence was measured by a fluorescence microscope (TE200U, Nikon), and the devices were connected to a potentiostat (CompactStat, Ivium) for electrochemical analysis.

ACKNOWLEDGMENTS. This work was supported by Samsung Research Funding Center of Samsung Electronics under Project SRFC-MA1402-11.

1. M. Kaltenbrunner *et al*., An ultra-lightweight design for imperceptible plastic electronics. *Nature* **499**, 458–463 (2013).
2. M. L. Hammock, A. Chortos, B. C. Tee, J. B. Tok, Z. Bao, 25th anniversary article: The evolution of electronic skin (e-skin): A brief history, design considerations, and recent progress. *Adv. Mater.* **25**, 5997–6038 (2013).
3. D. H. Kim *et al*., Stretchable and foldable silicon integrated circuits. *Science* **320**, 507–511 (2008).
4. C. Dagdeviren *et al*., Conformal piezoelectric energy harvesting and storage from motions of the heart, lung, and diaphragm. *Proc. Natl. Acad. Sci. U.S.A.* **111**, 1927–1932 (2014).
5. D. H. Kim, R. Ghaffari, N. Lu, J. A. Rogers, Flexible and stretchable electronics for biointegrated devices. *Annu. Rev. Biomed. Eng.* **14**, 113–128 (2012).
6. C. Pang, C. Lee, K. Y. Suh, Recent advances in flexible sensors for wearable and implantable devices. *J. Appl. Polym. Sci.* **130**, 1429–1441 (2013).
7. D. H. Kim *et al*., Dissolvable films of silk fibroin for ultrathin conformal bio-integrated electronics. *Nat. Mater.* **9**, 511–517 (2010).
8. J. Viventi *et al*., Flexible, foldable, actively multiplexed, high-density electrode array for mapping brain activity in vivo. *Nat. Neurosci.* **14**, 1599–1605 (2011).
9. N. Sinha *et al*., Predicting neurosurgical outcomes in focal epilepsy patients using computational modelling. *Brain* **140**, 319–332 (2017).
10. D. R. Kipke *et al*., Advanced neurotechnologies for chronic neural interfaces: New horizons and clinical opportunities. *J. Neurosci.* **28**, 11830–11838 (2008).
11. B. P. Timko *et al*., Electrical recording from hearts with flexible nanowire device arrays. *Nano Lett.* **9**, 914–918 (2009).
12. D. H. Kim *et al*., Materials for multifunctional balloon catheters with capabilities in cardiac electrophysiological mapping and ablation therapy. *Nat. Mater.* **10**, 316–323 (2011).
13. N. A. Peppas, J. Z. Hilt, A. Khademhosseini, R. Langer, Hydrogels in biology and medicine: From molecular principles to bionanotechnology. *Adv. Mater.* **18**, 1345–1360 (2006).
14. H. B. Zhang, J. K. Jackson, M. Chiao, Microfabricated drug delivery devices: Design, fabrication, and applications. *Adv. Funct. Mater.* **27**, 1703606 (2017).
15. S. Lin *et al*., Stretchable hydrogel electronics and devices. *Adv. Mater.* **28**, 4497–4505 (2016).
16. P. Fattahi, G. Yang, G. Kim, M. R. Abidian, A review of organic and inorganic biomaterials for neural interfaces. *Adv. Mater.* **26**, 1846–1885 (2014).
17. Y. W. Jiang, B. Z. Tian, Inorganic semiconductor biointerfaces. *Nat. Rev. Mater.* **3**, 473–490 (2018).
18. J. W. Jeong *et al*., Soft materials in neuroengineering for hard problems in neuroscience. *Neuron* **86**, 175–186 (2015).
19. D. T. Simon, E. O. Gabrielsson, K. Tybrandt, M. Berggren, Organic bioelectronics: Bridging the signaling gap between biology and technology. *Chem. Rev.* **116**, 13009–13041 (2016).
20. M. Asplund, T. Nyberg, O. Inganas, Electroactive polymers for neural interfaces. *Polym. Chem.* **1**, 1374–1391 (2010).
21. H. R. Lee, C. C. Kim, J. Y. Sun, Stretchable ionics - a promising candidate for upcoming wearable devices. *Adv. Mater.* **30**, e1704403 (2018).
22. T. A. Sjostrom *et al*., A decade of iontronic delivery devices. *Adv Mater Technol.* **3**, 1700360 (2018).
23. H. Chun, T. D. Chung, Iontronics. *Annu. Rev. Anal. Chem. (Palo Alto, Calif.)* **8**, 441–462 (2015).
24. J. Y. Sun *et al*., Highly stretchable and tough hydrogels. *Nature* **489**, 133–136 (2012).
25. C. Keplinger *et al*., Stretchable, transparent, ionic conductors. *Science* **341**, 984–987 (2013).
26. T. Ono, T. Sugimoto, S. Shinkai, K. Sada, Lipophilic polyelectrolyte gels as superabsorbent polymers for nonpolar organic solvents. *Nat. Mater.* **6**, 429–433 (2007).
27. H. Takahashi, K. Itoga, T. Shimizu, M. Yamato, T. Okano, Human neural tissue construct fabrication based on scaffold-free tissue engineering. *Adv. Healthc. Mater.* **5**, 1931–1938 (2016).
28. M. C. Darnell *et al*., Performance and biocompatibility of extremely tough alginate/polyacrylamide hydrogels. *Biomaterials* **34**, 8042–8048 (2013).
29. E. O. Gabrielsson, M. Berggren, Polyphosphonium-based bipolar membranes for rectification of ionic currents. *Biomicrofluidics* **7**, 64117 (2013).
30. J. H. Han, K. B. Kim, H. C. Kim, T. D. Chung, Ionic circuits based on polyelectrolyte diodes on a microchip. *Angew. Chem. Int. Ed. Engl.* **48**, 3830–3833 (2009).
31. O. J. Cayre, S. T. Chang, O. D. Velev, Polyelectrolyte diode: Nonlinear current response of a junction between aqueous ionic gels. *J. Am. Chem. Soc.* **129**, 10801–10806 (2007).
32. K. Tybrandt, K. C. Larsson, A. Richter-Dahlfors, M. Berggren, Ion bipolar junction transistors. *Proc. Natl. Acad. Sci. U.S.A.* **107**, 9929–9932 (2010).
33. K. Tybrandt, E. O. Gabrielsson, M. Berggren, Toward complementary ionic circuits: The npn ion bipolar junction transistor. *J. Am. Chem. Soc.* **133**, 10141–10145 (2011).
34. K. B. Kim, J.-H. Han, H. C. Kim, T. D. Chung, Polyelectrolyte junction field effect transistor based on microfluidic chip. *Appl. Phys. Lett.* **96**, 143506 (2010).
35. J. Rivnay *et al*., Organic electrochemical transistors. *Nat. Rev. Mater.* **3**, 17086 (2018).
36. K. Tybrandt, R. Forchheimer, M. Berggren, Logic gates based on ion transistors. *Nat. Commun.* **3**, 871 (2012).
37. H. B. Liu *et al*., Sensing minute changes in biological cell monolayers with THz differential time-domain spectroscopy. *Biosens. Bioelectron.* **22**, 1075–1080 (2007).
38. S. H. Chung, R. A. Kennedy, Forward-backward non-linear filtering technique for extracting small biological signals from noise. *J. Neurosci. Methods* **40**, 71–86 (1991).
39. R. F. Pierret, *Semiconductor Device Fundamentals* (Addison-Wesley, Reading, MA, 1996), p. xxiii, 792 pp.
40. J. H. Han *et al*., Ion flow crossing over a polyelectrolyte diode on a microfluidic chip. *Small* **7**, 2629–2639 (2011).
41. A. G. Volkov, S. Paula, D. W. Deamer, Two mechanisms of permeation of small neutral molecules and hydrated ions across phospholipid bilayers. *Bioelectrochem. Bioenerg.* **42**, 153–160 (1997).